

ELECTRON-ION RECOMBINATION ON GRAINS AND POLYCYCLIC AROMATIC HYDROCARBONS

JOSEPH C. WEINGARTNER

CITA, 60 St. George Street, University of Toronto, Toronto, ON M5S 3H8, Canada
weingart@cita.utoronto.ca

AND

B. T. DRAINE

Princeton University Observatory, Peyton Hall, Princeton, NJ 08544, USA
draine@astro.princeton.edu
Draft version April 26, 2024

ABSTRACT

With the high-resolution spectroscopy now available in the optical and satellite UV, it is possible to determine the neutral/ionized column density ratios for several different elements in a single cloud. Assuming ionization equilibrium for each element, one can make several independent determinations of the electron density. For the clouds for which such an analysis has been carried out, these different estimates disagree by large factors, suggesting that some process (or processes) besides photoionization and radiative recombination might play an important role in the ionization balance. One candidate process is collisions of ions with dust grains.

Making use of recent work quantifying the abundances of polycyclic aromatic hydrocarbon molecules and other grains in the interstellar medium, as well as recent models for grain charging, we estimate the grain-assisted ion recombination rates for several astrophysically important elements. We find that these rates are comparable to the rates for radiative recombination for conditions typical of the cold neutral medium. Including grain-assisted ion recombination in the ionization equilibrium analysis leads to increased consistency in the various electron density estimates for the gas along the line of sight to 23 Orionis. However, not all of the discrepancies can be eliminated in this way; we speculate on some other processes that might play a role. We also note that grain-assisted recombination of H⁺ and He⁺ leads to significantly lower electron fractions than usually assumed for the cold neutral medium.

Subject headings: dust—ISM: abundances—ISM: clouds—stars: individual (23 Orionis, HD 215733)

1. INTRODUCTION

The electron number density n_e in diffuse interstellar clouds is often inferred from the observed column densities of different ionization stages of metals. The assumption of ionization equilibrium yields

$$\Gamma(X^i)n(X^i) = \alpha_r(X^{i+1}, T)n_e n(X^{i+1}) \quad , \quad (1)$$

where $n(X^i)$ is the number density of the i -th ion of element X, $\Gamma(X^i)$ is the ionization rate for $X^i \rightarrow X^{i+1}$, and $\alpha_r(X^{i+1}, T)$ is the rate coefficient (which depends on the gas temperature T) for recombinations $X^{i+1} \rightarrow X^i$. It is usually assumed that radiative recombination is dominant at low temperatures; dielectronic recombination is often important when $T \gtrsim 10^4$ K.

The Goddard High Resolution Spectrograph on the *Hubble Space Telescope* has made possible the simultaneous determination of n_e through analysis of the ionization balance of several different metals. In some cases, the values of n_e inferred from different species differ by large factors (Fitzpatrick & Spitzer 1997; Welty et al. 1999), suggesting either that the ionization is far from a steady-state equilibrium or that another process (or processes) besides photoionization and radiative recombination affects the ionization balance.

One candidate process is ion recombination via electron transfer from a grain or molecule to the ion during a collision (Weisheit & Upham 1978; Omont 1986; Draine & Sutin 1987;

Lepp et al. 1988). The “removed” ion might remain in the gas phase (in a lower ionization stage) or it might be depleted from the gas altogether, if it sticks to the grain.¹ The grain-assisted ion removal rate is expected to vary from species to species since the possibility of charge transfer depends on the electron affinity of the ion and the collision rate depends on its mass.

The collision rate also depends on the grain charge and size; when the grain charge $Z \leq 0$, the ratio of the collision cross section to the geometric cross section is larger for smaller grains (Draine & Sutin 1987). Thus, a large population of molecules or very small grains with $Z \leq 0$ could contribute significantly to ion removal.

Observations of emission from the diffuse interstellar medium (ISM) have revealed features at 3.3, 6.2, 7.7, 8.6, and 11.3 μm (see Sellgren 1994 for a review), which have been identified as C—H and C—C stretching and bending modes in polycyclic aromatic hydrocarbons (PAHs; Léger & Puget 1984; Allamandola, Tielens, & Barker 1985). Li & Draine (2001) compared observations of diffuse Galactic emission with detailed model calculations for PAHs heated by Galactic starlight and found that a C abundance² $\sim 4\text{--}6 \times 10^{-5}$ is required in hydrocarbon molecules with $\lesssim 10^3$ C atoms.³ In recent charging models, PAHs are found to be predominantly neutral in the diffuse ISM (Bakes & Tielens 1994; Weingartner & Draine 2001b).

In §2, we estimate grain-assisted ion removal rates for sev-

¹ Henceforth, we will include molecules in the “grain” population.

² By “abundance” we mean the number of atoms of an element per interstellar H nucleus.

³ Electric dipole emission from this population can account for the dust-correlated component of the diffuse Galactic microwave emission (Draine & Lazarian 1998; Draine & Li 2001).

eral metals, employing a grain size distribution that (a) includes PAHs in numbers sufficient to account for the observed infrared and microwave emission and (b) reproduces the observed extinction of starlight (Weingartner & Draine 2001a). In §3, we compare the grain-assisted ion removal rate with the radiative recombination rate, finding them to be comparable in the cold neutral medium. In §4, we discuss the determination of electron densities from observed column density ratios when grain-assisted ion removal is important. In §5, we apply these results to two observed lines of sight. We find that the inclusion of grain-assisted ion removal cannot, on its own, reconcile the electron densities inferred from different species observed towards 23 Ori. In §6, we speculate on additional processes that might affect ionization balance along this line of sight. In §7, we investigate the impact of grain-assisted ion recombination on the electron fraction in the cold neutral medium. We summarize our conclusions in §8.

2. ION REMOVAL RATES

Consider the collision of an ion X^i with a dust grain of radius a and charge Ze (e is the proton charge). We assume that an electron is transferred from the grain to the ion if $\text{IP}(a, Z) < \text{IP}(X^{i-1})$, where $\text{IP}(a, Z)$ is the grain ionization potential and $\text{IP}(X^{i-1})$ is the ionization potential of X^{i-1} (equal to the electron affinity of X^i ; see Table 1 for our adopted values). This is certainly an oversimplification since the electrostatic energy of the grain-ion combination usually increases following electron transfer. However, it is not clear how to evaluate the electrostatic energy when the distance from the grain to the ion is \lesssim a few angstroms. Thus, our estimates for ion removal rates should be regarded as likely upper limits. Below, we will estimate the extent to which these rates might be changed if the electrostatic energy changes were included in the analysis.

We adopt the following expression for the ion removal rate:

$$\frac{dn_i}{dt} = - \int dn_{\text{gr}} \sum_Z f(a, Z) J_i(Z) \theta[\text{IP}(X^{i-1}) - \text{IP}(a, Z)] \quad , \quad (2)$$

where n_i is the number density of X^i , $n_{\text{gr}}(a)$ is the number density of grains with radii $\leq a$, $f(a, Z)$ is the fraction of the grains of radius a that have charge Ze , and $\theta(y) = 0$ if $y < 0$ and 1 if $y \geq 0$. Ions arrive at a grain with size a and charge Z at the rate

$$J_i(Z) = n_i \left(\frac{8kT}{\pi m_p} \right)^{1/2} A_X^{-1/2} \pi a^2 \tilde{J}(\tau_i \equiv akT/q_i^2, \xi_i \equiv Ze/q_i) \quad , \quad (3)$$

where k is Boltzmann's constant, m_p is the proton mass, A_X is the ion mass number, q_i is the ion charge, and expressions for the dimensionless function $\tilde{J}(\tau_i, \xi_i)$ are given in Draine & Sutin (1987).

Grain charge distributions in the diffuse ISM are set primarily by the balance between electron loss via photoelectric emission versus electron gain via accretion from the gas. We calculate the steady-state charge distributions $f(a, Z)$ using the charging algorithm given by Weingartner & Draine (2001b) and the average interstellar radiation field (ISRF) spectrum for the solar neighborhood as estimated by Mezger, Mathis, & Panagia (1982) and Mathis, Mezger, & Panagia (1983). An often-used measure of the radiation intensity is the parameter $G \equiv u_{\text{rad}}^{\text{uv}}/u_{\text{Hab}}^{\text{uv}}$, where $u_{\text{rad}}^{\text{uv}}$ is the energy density in the radiation field between 6 eV and 13.6 eV and $u_{\text{Hab}}^{\text{uv}} = 5.33 \times 10^{-14} \text{ erg cm}^{-3}$ is the Habing (1968) estimate of the starlight energy density in

this range.⁴ For the ISRF, $G = 1.13$. Grain charging is largely determined by the parameter

$$\psi \equiv G\sqrt{T}/n_e \quad (4)$$

(Bakes & Tielens 1994; Weingartner & Draine 2001b), with only a weak additional dependence on T . Examples of charge distribution functions $f(a, Z)$ are given in Weingartner & Draine (2001b).

We define a rate coefficient $\alpha_g(X^i, \psi, T)$ for electron transfer to ion X^i due to collisions with grains by

$$\frac{dn_i}{dt} = -\alpha_g(X^i, \psi, T) n_i n_{\text{H}} \quad , \quad (5)$$

where n_{H} is the H nucleus number density. In Figure 1, we display α_g as a function of ψ for several ions X^i and $T = 100 \text{ K}$. In Figure 1, and throughout this paper, we employ the grain size distribution from Weingartner & Draine (2001a) with $R_V = 3.1$ and $b_C = 6 \times 10^{-5}$ (their favored distribution for the average diffuse ISM). Note that α_g decreases sharply as ψ increases, i.e., as the average grain charge increases. When $T \lesssim 10^3 \text{ K}$, the dependence of α_g on T is quite mild since, for neutral grains and $\tau_i \ll 1$, $\tilde{J} \propto T^{-1/2}$, cancelling the factor of $T^{1/2}$ in equation (3).

For the cases illustrated in Figure 1, we have also computed a modified ion removal rate coefficient α'_g , for which we apply a different criterion for electron transfer:

$$\text{IP}(a, Z) - \text{IP}(X^{i-1}) + \Delta U(Z, i) < 0 \quad . \quad (6)$$

Here, ΔU is the change in the interaction energy between the grain and the ion due to the electron transfer. We approximate (see Appendix)

$$\Delta U(Z, z) \approx (z - Z - 1) \frac{e^2}{(a + r_0)} + \frac{(2z - 1)e^2 a^3}{2r_0(a + r_0)^2(2a + r_0)} \quad , \quad (7)$$

where Ze is the initial grain charge, ze is the initial ion charge, and r_0 is the atomic radius (see Table 1 for our adopted values of r_0). Since the distance of closest approach between the ion and the grain surface is unknown, we have taken it to be equal to the atomic radius.

The first term in equation (7) is the monopole contribution due to the net charges on the grain and ion. Since the grains are predominantly neutral ($Z = 0$) and most ions of interest are singly ionized ($z = 1$), the inclusion of this term usually has a negligible effect on the calculated ion removal rate. The second term in equation (7) is due to the polarization of the grain by the ion. Our classical calculation of the interaction energy assumes that the grain is (a) a perfect conductor and (b) a sphere with a perfectly sharp surface. These assumptions can lead to substantial errors in the estimate of the image potential when the ion-grain surface separation \leq a few angstroms. We have neglected the dipole moment in the atom or ion induced by the grain charge, since the approximation of the atom/ion dipole as a point dipole breaks down when the distance from the atom/ion to the grain surface is comparable to the size of the atom—the case of interest here.

In Figure 2, we display α'_g/α_g . For cold and warm neutral medium conditions, α'_g/α_g is generally ~ 1 ; thus, it appears that, for most cases of interest, an accurate accounting of the increase in electrostatic energy following electron transfer would not substantially reduce the computed ion removal rate.

For a given ion, α_g can be represented approximately by the following fitting formula:

$$\alpha_g(X^i, \psi, T) \approx \frac{10^{-14} C_0 \text{ cm}^3 \text{ s}^{-1}}{1 + C_1 \psi^{C_2} [1 + C_3 T^{C_4} \psi^{-C_5 - C_6 \ln T}]} \quad , \quad (8)$$

⁴ For comparison, the interstellar radiation field estimated by Draine (1978) has $u = 8.93 \times 10^{-14} \text{ erg cm}^{-3}$ between 6 and 13.6 eV, or $G = 1.68$.

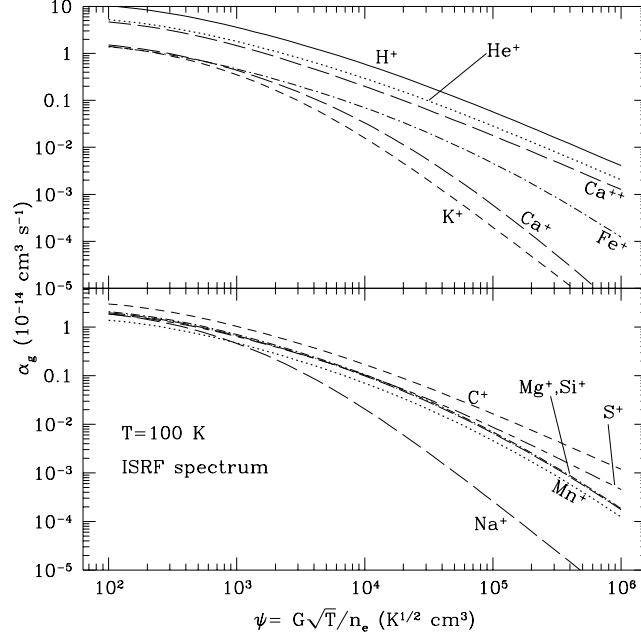


FIG. 1.— Rate coefficient α_g for grain-assisted removal of selected ions as a function of the charging parameter ψ , for the ISRF spectrum and gas temperature $T = 100\text{K}$.

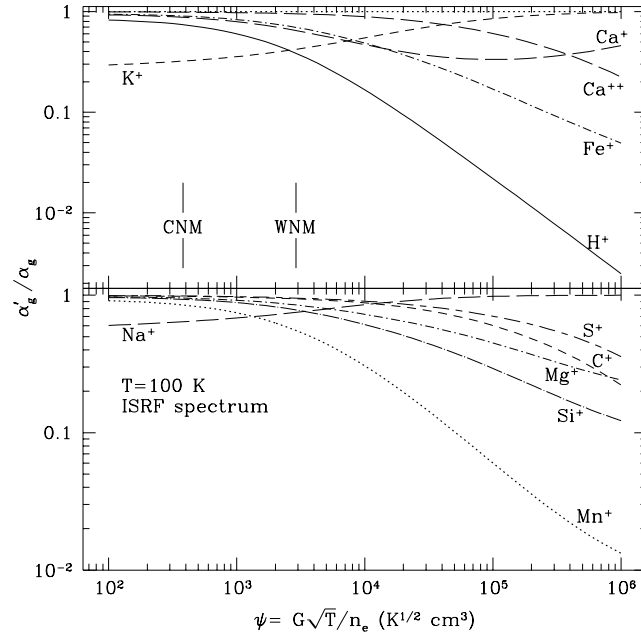


FIG. 2.— α'_g/α_g , where α'_g is computed assuming a more stringent criterion for the transfer of an electron from grain to ion, in which the increase in electrostatic energy due to the interaction of the grain and ion charge is taken into account in an approximate manner. Nominal cold and warm neutral medium conditions are indicated (“CNM” and “WNM”, respectively).

with T in kelvins and ψ in units of $\text{K}^{1/2}\text{cm}^3$; values of the fitting coefficients C_0 – C_6 are given in Table 2 for selected ions.⁵ Approximation (8) is accurate to within 20% when $10 \leq T \leq 10^3\text{K}$ and $10^2 \leq \psi \leq 10^6\text{K}^{1/2}\text{cm}^3$. In the grain-assisted recombination of Ca^{2+} , there is a possibility for two electrons to be transferred to the ion, resulting in Ca^0 . We assume that this occurs in a two-step process and that the energy released following the first electron transfer is dissipated into

heat, and thus is not available to assist in the second transfer. With these assumptions, the criterion for double electron transfer is

$$\text{IP}(a, Z+1) < \text{IP}(\text{Ca}^0) \quad (9)$$

For this criterion, $10 \leq T \leq 10^3\text{K}$, and $10^2 \leq \psi \leq 10^6\text{K}^{1/2}\text{cm}^3$, the probability of double charge transfer can be approximated

⁵ A FORTRAN subroutine implementing approximation (8) is available on the World Wide Web at www.cita.utoronto.ca/~weingart.

to within 10% by

$$f_{\text{Ca}^{++} \rightarrow \text{Ca}^0} \approx \frac{0.415}{1 + 6.38 \times 10^{-5} \psi^{1.252} (1 + 3.57 \times 10^{-6} \psi^{1.124})} . \quad (10)$$

Note, however, that the double electron transfer rate could be dramatically reduced if electrostatic energy changes (as in eq. [7]) are included in the criterion for electron transfer.

3. GRAIN-ASSISTED ION REMOVAL VERSUS RADIATIVE RECOMBINATION

To gauge the importance of grain-assisted ion removal in the diffuse ISM, we plot in Figures 3 and 4 a critical electron fraction

$$x_{\text{crit}}(\text{X}^i, \psi, T) \equiv \frac{\alpha_g(\text{X}^i, \psi, T)}{\alpha_r(\text{X}^i, T)} ; \quad (11)$$

if $x \equiv n_e/n_{\text{H}} \leq x_{\text{crit}}$, then grain-assisted removal of X^i occurs more rapidly than radiative recombination to X^{i-1} . We use the FORTRAN routine `rrfit.f` to evaluate radiative recombination coefficients.⁶ In Figure 3, we take $T = 100\text{K}$, appropriate for the cold neutral medium (CNM). For a nominal CNM electron fraction $x \approx 10^{-3}$ and $\psi \approx 400\text{K}^{1/2}\text{cm}^3$, the grain-assisted ion removal rate is generally comparable to the radiative recombination rate and therefore will appreciably affect the ionization balance for H^+ and most metal ions.

In Figure 4, we take $T = 6000\text{K}$, appropriate for the warm neutral medium (WNM) and warm ionized medium (WIM). Adopting $x \approx 0.1$ and $\psi \approx 3000\text{K}^{1/2}\text{cm}^3$ for the WNM, we find that the grain-assisted ion removal rate $\lesssim 10\%$ the radiative recombination rate. For the WIM ($x \approx 1$, $\psi \approx 1000\text{K}^{1/2}\text{cm}^3$), grain-assisted ion removal contributes at most at the few percent level.

4. ELECTRON DENSITY DETERMINATIONS INCLUDING GRAIN-ASSISTED ION REMOVAL

When grain-assisted ion removal is important, the ionization balance equation (1) must be replaced with the following set of equations:

$$\frac{dn_{i+1}}{dt} = \Gamma(\text{X}^i)n_i - \alpha_r(\text{X}^{i+1})n_en_{i+1} - \alpha_g(\text{X}^{i+1})n_{\text{H}}n_{i+1} \quad (12)$$

and

$$\frac{dn_i}{dt} = -\Gamma(\text{X}^i)n_i + \alpha_r(\text{X}^{i+1})n_en_{i+1} + \alpha_g(\text{X}^{i+1})n_{\text{H}}n_{i+1}(1-s) , \quad (13)$$

where s is the probability that an ion sticks to a grain following charge exchange.⁷ Of course, if more than two ionization stages are populated, then more equations are needed. When $s > 0$, n_i and n_{i+1} both decay, but, with the exception of transients that die out rapidly, the ratio n_{i+1}/n_i is constant:

$$\frac{n_{i+1}}{n_i} \approx \frac{q}{2b} \left[1 + \left(1 + \frac{4b}{q^2} \right)^{1/2} \right] , \quad (14)$$

where $b \equiv r_1 + r_2(1-s)$, $q \equiv 1 - r_1 - r_2$, $r_1 \equiv \alpha_r n_e / \Gamma$, and $r_2 \equiv \alpha_g n_{\text{H}} / \Gamma$.

Solving equation (14) for n_e in terms of the observed column density ratio $R \equiv n(\text{X}^i)/n(\text{X}^{i+1})$, we find

$$n_e = \frac{R\Gamma}{\alpha_r} \left[1 - \frac{1-s+R}{1+R} \frac{\alpha_g n_{\text{H}}}{R\Gamma} \right] . \quad (15)$$

⁶ The subroutine `rrfit.f` was written by D. A. Verner and is available on the World Wide Web at www.pa.uky.edu/~verner/fortran.html.

⁷ We assume that ions do not stick to grains following collisions without charge exchange.

Since α_g depends on n_e (through its dependence on the charging parameter ψ), equation (15) must be solved iteratively, but generally converges rapidly. Usually $r_1 \ll 1$ and $r_2 \ll 1$ (implying $R \ll 1$). Thus, the impact of grain-assisted ion removal on the electron density determination decreases as the sticking probability $s \rightarrow 1$. The observed interstellar depletions vary widely from element to element, implying $s \ll 1$ for some elements (e.g. S) while $s \sim 1$ for others (e.g. Ti, Ca; see Weingartner & Draine 1999). This wide variation in s could also lead to discrepancies in electron density estimates when different elements are observed.

A large fraction of the Ca in diffuse clouds can be in Ca^{++} ; thus, we must consider the ionization equilibrium of a 3-level system in this case. For arbitrary s , this results in a rather complicated cubic equation for n_e in terms of the observed ratio $R_1 \equiv n(\text{Ca}^0)/n(\text{Ca}^+)$. However, the equation simplifies to a quadratic when $s = 0$ or $s = 1$. Before displaying the results, it is convenient to introduce some notation: $\tilde{n}_e \equiv R_1 \Gamma(\text{Ca}^0)/\alpha_r(\text{Ca}^+)$ (this is the value of n_e when grains are unimportant), $g_1 \equiv \alpha_g(\text{Ca}^+)/\alpha_r(\text{Ca}^+)$, $g_2 \equiv \alpha_g(\text{Ca}^{++})/\alpha_r(\text{Ca}^{++})$, $d \equiv \alpha_r(\text{Ca}^{++})/\alpha_r(\text{Ca}^+)$, $\gamma \equiv \Gamma(\text{Ca}^+)/\Gamma(\text{Ca}^0)$, $h_1 \equiv \alpha_g(\text{Ca}^+)n_{\text{H}}/\alpha_r(\text{Ca}^+)\tilde{n}_e$, $h_2 \equiv \alpha_g(\text{Ca}^{++})n_{\text{H}}/\alpha_r(\text{Ca}^+)\tilde{n}_e$, and $f_2 \equiv f_{\text{Ca}^{++} \rightarrow \text{Ca}^0}$ (from eq. 10).

When $s = 0$,

$$n_e = \frac{1}{2}(\tilde{n}_e - g_1 n_{\text{H}})(1 + Q_0) - \frac{1}{2}g_2 n_{\text{H}}(1 - Q_0) , \quad (16)$$

where

$$Q_0 = \left\{ 1 - \frac{4g_2 n_{\text{H}} \gamma f_2 \tilde{n}_e}{R_1 [(g_1 - g_2)n_{\text{H}} - \tilde{n}_e]^2} \right\}^{1/2} . \quad (17)$$

Note that equation (16) reduces to equation (15) when $\gamma = 0$ or $f_2 = 0$. The ratio $R_2 \equiv n(\text{Ca}^0)/n(\text{Ca}^{++})$ is given by

$$R_2 = \frac{R_1^2}{\gamma} \left(h_2 + d \frac{n_e}{\tilde{n}_e} \right) . \quad (18)$$

When $s = 1$,

$$n_e = \tilde{n}_e \left[1 - \frac{R_1 h_1 (1 + dR_1)(1 + Q_1) + R_1 (d + h_2)(1 + R_1)(1 - Q_1) + \gamma}{2(1 + R_1)(1 + dR_1)} \right] , \quad (19)$$

where

$$Q_1 = \left(1 + \frac{\gamma^2 + 2\gamma R_1 \{ h_1(1 + dR_1) + (1 + R_1)[d - h_2(1 + 2dR_1)] \}}{R_1^2 [h_1(1 + dR_1) - (d + h_2)(1 + R_1)]^2} \right)^{1/2} ; \quad (20)$$

$$R_2 = \frac{R_1^2}{\gamma} \left[h_2 - R_1^{-1} + (d + R_1^{-1}) \frac{n_e}{\tilde{n}_e} \right] . \quad (21)$$

Note that equation (19) reduces to equation (15) when $\gamma = 0$.

5. APPLICATION TO OBSERVATIONS

5.1. HD 215733

Fitzpatrick & Spitzer (1997) performed ionization equilibrium analyses of $\text{Ca}^+/\text{Ca}^{++}$, C^0/C^+ , Mg^0/Mg^+ , and S^0/S^+ for several clouds along the line of sight to HD 215733. In the case of Ca^+ , the Ca^{++} abundance was estimated based on an assumed gas-phase Ca abundance. In Table 3, we reproduce their inferred temperatures and H number densities for the cold

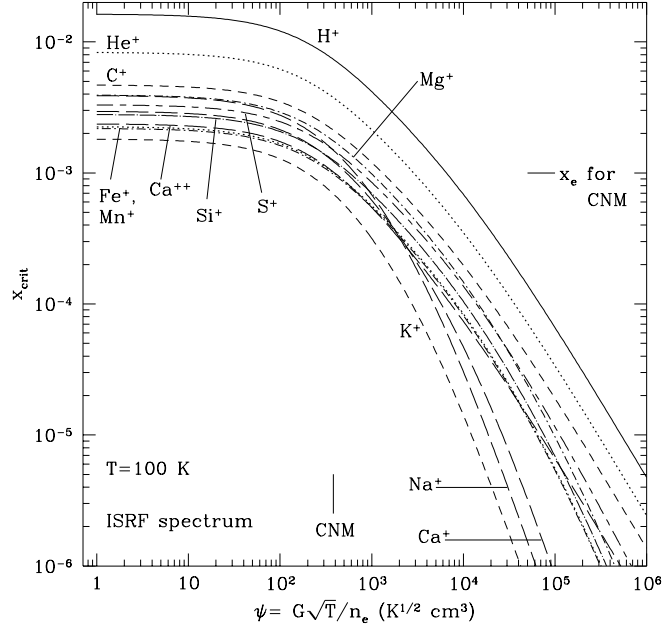


FIG. 3.— Critical electron fraction: if $x \leq x_{\text{crit}}$, then the indicated ion is removed more effectively via collisions with grains than via radiative recombination. The ticks labeled “CNM” are for canonical cold neutral medium values of ψ and x .

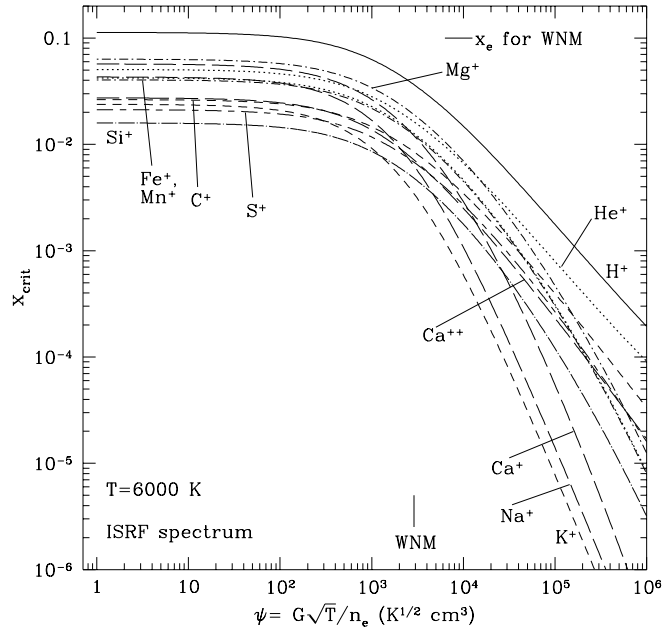


FIG. 4.— Same as Figure 3, except for $T = 6000\text{K}$ instead of $T = 100\text{K}$. The ticks labeled “WNM” are for canonical warm neutral medium values of ψ and x .

cloud components. In the upper panel of Figure 5, we reproduce their electron density determinations.⁸ The electron densities inferred from the C and Mg abundance ratios appear to be roughly consistent, but those inferred from the Ca abundance ratios are systematically lower.

In the lower panel of Figure 5, we display revised n_e determinations that take grain-assisted ion removal into account. We assume $s \approx 1$ for Ca, which is observed to be highly depleted

in cold clouds, and $s \approx 0$ for C, Mg, and S, which are not as severely depleted. With this modification, the Mg determinations lie between the C and Ca determinations, and are consistent with both. The C and Ca determinations remain inconsistent. If dissociative recombination of CH^+ is important in these clouds, then the n_e inferred from the C abundance ratios are too high; unfortunately, the CH^+ column density towards HD 215733 is not known. Alternatively, the n_e inferred from the

⁸ The Mg^+ f-values used by Fitzpatrick & Spitzer (1997) are apparently too large by a factor of ≈ 2.4 (Fitzpatrick 1997). Thus, we have multiplied the n_e values obtained from the Mg column density ratio by 2.4.

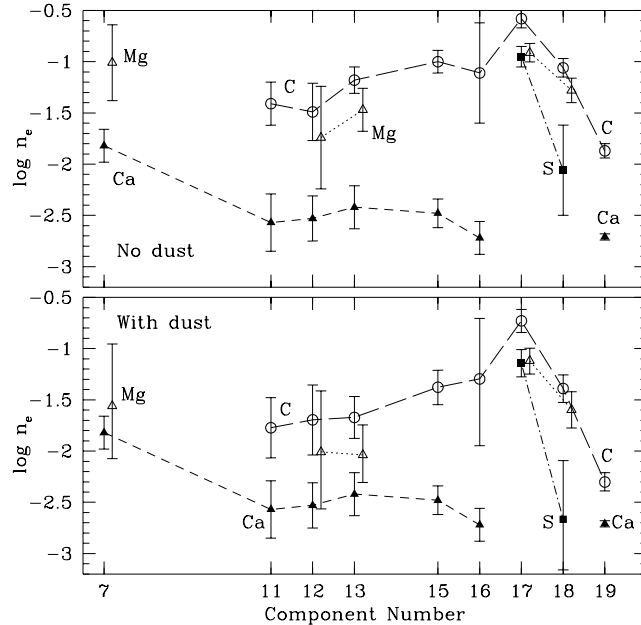


FIG. 5.— Upper panel: Fitzpatrick & Spitzer (1997) results for n_e (in cm^{-3}) for cool cloud components along the line of sight to HD 215733, with n_e determined from ionization equilibrium for Ca^+ , C^0 , Mg^0 , and S^0 (Mg results are adjusted as per Fitzpatrick 1997). Lower panel: Modified n_e determinations, with grain-assisted ion removal included. We assume $s = 1$ for Ca and $s = 0$ for C, Mg, and S.

Ca abundance ratios could be too small, as would be the case if the Ca abundance has been overestimated. Unfortunately, with only three elements for which both ionization stages have been observed, it is difficult to arrive at definitive conclusions regarding the electron densities in many of these components.

5.2. 23 Ori

Welty et al. (1999, hereafter W99) have conducted a detailed investigation of the diffuse clouds along the line of sight to 23 Orionis. They inferred $T \sim 100\text{K}$, $n_{\text{H}} \sim 10\text{cm}^{-3}$, and $N_{\text{H}} \approx 5 \times 10^{20}\text{cm}^{-2}$ for the cold cloud material along this sightline at heliocentric velocities $20 < v_{\odot} < 27\text{km s}^{-1}$. They also inferred n_e using equation (1) for ionization equilibrium (between X^0 and X^+) with several different elements, and found widely varying values; we display their electron densities as open triangles in Figure 6.⁹ The electron densities inferred if ionization equilibrium is assumed vary over about an order of magnitude, depending on which element is used.

Electrons will collisionally excite the $^2\text{P}_{3/2}$ excited fine structure levels of C^+ and Si^+ . W99 report $N(\text{C}^+) = 10^{16.95}\text{cm}^{-2}$, and $N(\text{C}^{+*}) < 10^{15.0}\text{cm}^{-2}$, from which we infer $n_e < 0.075\text{cm}^{-3}$; we assumed $T = 100\text{K}$, a collision strength $\Omega = 2.1$ from Keenan et al. (1986) and H collisional rates from Launay & Roueff (1977).

For Si^+ , W99 find $N(\text{Si}^+) = 10^{15.37}\text{cm}^{-2}$ and $N(\text{Si}^{+*}) < 10^{10.7}\text{cm}^{-2}$, from which we find $n_e < 0.12\text{cm}^{-3}$, assuming a collision strength $\Omega = 5.74$ (Keenan et al. 1985). H collisional rates have not been calculated; we use the rate coefficient calculated by Launay & Roueff for deexcitation of $\text{C}^+(^2\text{P}_{3/2})$.

Upper limits on n_e derived from fine-structure excitation are shown in Figure 6.

The electron densities inferred from ionization equilibrium

including grain-assisted ion removal are displayed as filled triangles in Figure 6. We have assumed $s = 0$ in order to maximize the effect that grain-assisted ion removal might have. (For most of the elements in Figure 6, this assumption seems reasonable. For Fe and Ca, however, the large depletions observed in interstellar gas suggest that $s \gtrsim 0.1$.) The W99 electron densities inferred using C, Na, Mg, and K are particularly large; the resulting n_e/n_{H} are high enough that the inclusion of grain-assisted ion removal does not dramatically alter the inferred values of n_e . Thus, the various n_e determinations do not appear to be reconciled by including this process.

However, some of the W99 n_e determinations might be too high for other reasons. Dissociative recombination of CH^+ might be an important additional recombination mechanism for C. W99 found that if the CH^+ observed towards 23 Ori resides in the cold cloud for which the C^0 and C^+ column densities were measured, then the estimated n_e must be revised downward from 0.26 to 0.04cm^{-3} (open square in Figure 6); of course, grain-assisted ion removal would reduce it further (filled square).

Na^+ and K^+ are unobservable since they have no resonance lines below the Lyman limit. Thus, W99 had to assume gas-phase Na and K abundances in order to analyze the ionization balance for these elements. W99 assumed depletions of 0.5 dex (relative to solar) for both elements. If, instead, these elements are assumed to be undepleted, then the n_e estimates are substantially smaller; these are indicated in Figure 6 by filled (open) squares for analyses that do (do not) include grain-assisted ion removal.

Note that Welty & Hobbs (2001) argue, on the basis of a large number of observed sight lines, that Na and K are generally depleted from the gas phase by 0.6–0.7 dex relative to solar. We consider the depletion estimates for Na and K to be quite uncer-

⁹ We display the W99 n_e determinations using photoionization rates for the “WJ1” radiation field (see Table 1); these photoionization rates are very similar to those for the ISRF of Mathis et al. (1983).

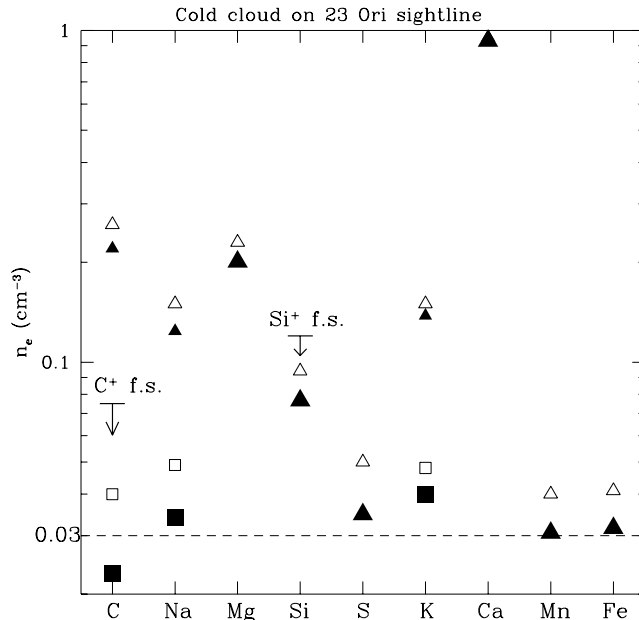


FIG. 6.— Electron density n_e inferred from ionization equilibrium for the cold gas towards 23 Orionis. Open triangles: Welty et al. (1999) analysis; Filled triangles: Welty et al. (1999) analysis plus grain-assisted ion removal; Open squares: Modified analysis (see text), without grain-assisted ion removal; Filled squares: Modified analysis, including grain-assisted ion removal. For each species, our favored n_e determination is indicated by an enlarged symbol. Our actual favored $n_e \approx 0.03 \text{ cm}^{-3}$ is indicated by the dashed line. Upper limits from the observed fine structure excitation from C^+ and Si^+ are also indicated.

tain, as they rely on knowledge of the electron density (which, as we have seen, is uncertain since “standard” ionization analyses give discrepant results when multiple elements are used).

If the revisions described above (for C, Na, and K) are correct, then the observed column densities for six elements (C, Na, S, K, Mn, Fe) yield $n_e \approx 0.03 \text{ cm}^{-3}$, consistent with the upper limits $n_e < 0.075 \text{ cm}^{-3}$ and $n_e < 0.12 \text{ cm}^{-3}$ obtained from the fine structure excitation of C^+ and Si^+ . For $n_e/n_{\text{H}} = 3 \times 10^{-3}$, grain-assisted ion removal contributes significantly to the recombination.

However, discrepancies remain for three elements: Ca, Mg, and Si.

1. W99 found $n_e \approx 0.95 \text{ cm}^{-3}$ from Ca^0/Ca^+ ionization balance. Using equation (16), we find $n_e = 0.93 \text{ cm}^{-3}$ even if $s = 0$, so including recombination on grains does not resolve this discrepancy.
2. Even after allowing for grain recombination with $s = 0$, the Mg^0/Mg^+ abundance ratio implies an electron density $n_e \approx 0.2 \text{ cm}^{-3}$ —a factor of 6 greater than our best estimate.
3. Even after allowing for grain recombination with $s = 0$, the Si^0/Si^+ abundance ratio implies an electron density $n_e \approx 0.08 \text{ cm}^{-3}$ —a factor of 2.5 greater than our best estimate.

Unless the photoionization rates have for some reason been overestimated, the observations suggest that additional physical processes are involved for these three elements.

6. POSSIBLE ADDITIONAL PROCESSES AFFECTING IONIZATION BALANCE IN 23 ORI

6.1. Dust Destruction?

In Figure 7, we plot the inferred electron density, normalized to our favored value of 0.03 cm^{-3} , versus the gas-phase element abundance in the cold cloud towards 23 Ori, normalized to the standard cold cloud abundance (see Table 5 in W99). We have included two points for Fe, with sticking coefficient $s = 0$ and $s = 1$; Fe is generally strongly depleted in cold clouds, suggesting that the sticking coefficient may be ~ 1 . Figure 7 shows a clear trend: greater neutral abundance enhancements are observed for elements with greater overall abundance enhancements. The total gas-phase abundances of Na and K are not known, but if they are enhanced by ≈ 0.4 dex over their standard values, then they fit the trend nicely. (We have also included points for Na and K for which the gas-phase abundance is enhanced by 0.1 dex, as assumed by W99, and by 0.6 dex, as assumed by us above. Neither of these choices lie close to the trend.) The observed correlation suggests the possibility that the enhanced neutral Mg, Si, and Ca abundances result from ongoing destruction of dust containing these elements, with the atoms injected into the gas as neutrals. However, the production rate of neutrals due to dust destruction would have to exceed the rate due to recombination; it is hard to imagine how such rapid dust destruction could be occurring. It seems to us unlikely that dust destruction is affecting the ionization balance observed toward 23 Ori.

6.2. Dielectronic Recombination?

It is intriguing to note that Mg^0 ($3s^2$ ground state), Si^0 ($3p^2$ ground state), and Ca^0 ($4p^2$ ground state) are all species for which dielectronic recombination is important for $T < 10^4 \text{ K}$; the dielectronic recombination rate for $\text{Mg}^+ \rightarrow \text{Mg}^0$ exceeds the radiative recombination rate for $T > 5800 \text{ K}$. W99 argue for a temperature $T \approx 100 \text{ K}$ for this velocity component, but perhaps there is some gas in this velocity range with $5000 \lesssim T \lesssim 10^4 \text{ K}$ and a relatively high electron density, leading to preferential

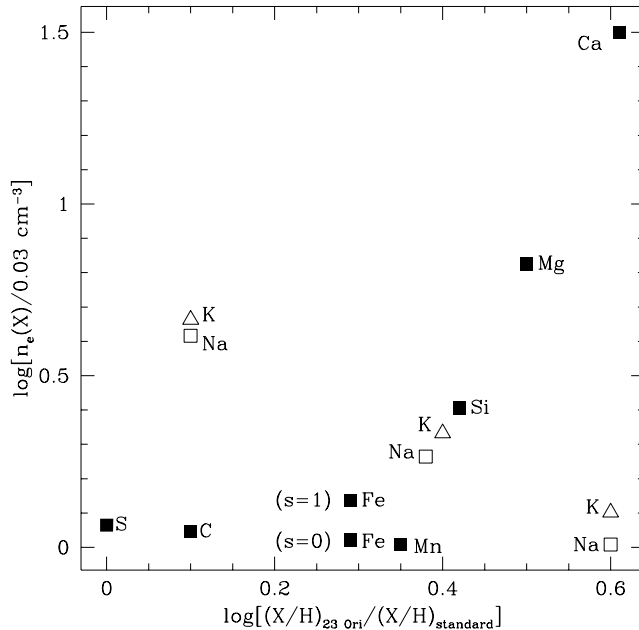


FIG. 7.— Electron density for the cold cloud along the line of sight to 23 Ori inferred from observed value of $N(X^0)/N(X^+)$, normalized to our favored value of 0.03 cm^{-3} , versus the factor by which the gas-phase element abundance is observed to be enhanced above its “standard” cold cloud value. The Na and K depletions are unknown, so for these elements we display a few possible points. The location of the Mn point is uncertain since W99 report only a marginal detection of Mn^0 .

recombination of those species with the largest (radiative + dielectronic) rate coefficients at these temperatures. It is also intriguing to note that W99 report detection of Al^{++} at the velocity of the dominant neutral absorption, suggesting that some of the material in this velocity range may be photoionized by photons beyond the Lyman limit, with accompanying ionization of H and presumably enhanced values of n_e and temperatures $T \approx 10^4\text{ K}$. Recall that CH^+ is present in this velocity range. The origin of interstellar CH^+ remains unclear, but all current scenarios for CH^+ formation, whether in MHD shock waves (Draine & Katz 1986; Pineau des Forêts et al. 1986), turbulent boundary layers of clouds (Duley et al 1992), strong Alfvén waves (Federman et al. 1996), or intermittent dissipation of turbulence (Falgarone, Pineau des Forêts, & Roueff 1995; Joulain et al. 1998), involve regions of enhanced temperature.

We have found that if $\approx 10\%$ of the column density arises in a warm component with $T \approx 10^4\text{ K}$ and $n_e \approx 4\text{ cm}^{-3}$, then the predicted column density ratios for all of the elements in Figure 6 are within a factor of ≈ 2 of the observed ratios. In this case, however, the predicted populations of the excited fine structure levels of C^+ and Si^+ substantially exceeds the observational upper limits (see §3.3.3 of W99). We were unable to find any models for which (a) dielectronic recombination in warm gas significantly increases the neutral/ionized column density ratios of Mg, Si, and Ca and (b) fine structure levels are not overpopulated. We conclude that dielectronic recombination cannot explain the observed high values of Mg^0/Mg^+ , Si^0/Si^+ , and Ca^0/Ca^+ .¹⁰

6.3. Chemistry?

W99 suggested that $n_e \approx 0.15\text{ cm}^{-3}$ in the cold gas towards 23 Ori and that charge exchange with protons might be an important ionization mechanism for S, Mn, and Fe, account-

ing for the lower n_e inferred from these species. W99 noted that charge transfer rates for $T \approx 100\text{ K}$ have not been calculated for these elements with protons, although potential energy curves calculated for SH^+ (Kimura et al. 1997) imply that the rate coefficient for $\text{S} + \text{H}^+ \rightarrow \text{S}^+ + \text{H}$ is very small at low temperatures, so that protons would not affect the S^0/S^+ ionization balance. It should also be noted that with the limit $n_e \lesssim 0.075\text{ cm}^{-3}$ from C^+ fine structure excitation, the charge transfer ionization rates $n(\text{H}^+)\langle\sigma v\rangle \lesssim 2 \times 10^{-10}\text{ s}^{-1}$ for Mn and Fe since $\langle\sigma v\rangle \lesssim 3 \times 10^{-9}\text{ cm}^3\text{ s}^{-1}$ even if MnH^+ or FeH^+ have favorable potential energy curves. Charge transfer with protons is therefore at most comparable to photoionization for Mn and Fe (see Table 1), so that n_e inferred from Mn and Fe cannot be raised by more than a factor of 2 even if charge transfer with protons is maximally effective. We therefore believe that the electron densities inferred from S, Mn, and Fe are reliable.

It is intriguing to note that the three atoms with np^2 ground states [$\text{C}(2p^2)$, $\text{Si}(3p^2)$, and $\text{Ca}(4p^2)$] are all overabundant. In the case of C we can attribute the overabundance to dissociative recombination of CH^+ , and the question arises whether dissociative recombination of SiH^+ and CaH^+ might also be taking place. CH^+ is believed to be produced by the exchange reaction $\text{C}^+ + \text{H}_2 + 0.40\text{ eV} \rightarrow \text{CH}^+ + \text{H}$. The reaction $\text{X}^+ + \text{H}_2 \rightarrow \text{XH}^+ + \text{H}$ is much more endothermic for Si⁺ (1.29 eV) than for C⁺ (0.40 eV). While the scenario for CH^+ formation remains unclear, the increased endothermicity for Si (and presumably for Ca, though the heat of formation of CaH^+ is unavailable) makes such a chemical explanation appear unlikely. Furthermore, production of SH^+ would appear more favorable than, say, SiH^+ , yet the observed S^0/S^+ ratio can be understood without invoking dissociative recombination of SH^+ .

¹⁰ W99 also conclude that dielectronic recombination is not likely to be responsible for the enhanced Ca^0/Ca^+ . They note that the n_e derived from Ca^0/Ca^+ are often higher than those derived from other neutral/ionized ratios, but that the line widths of Ca^0 usually indicate an origin in cool gas.

6.4. Atomic Physics?

The overabundance of the np^2 species suggests that some common atomic physics might be involved. If, for example, photoionization rates have been overestimated, or radiative recombination rates at $T \approx 100$ K have been underestimated, the rates for all three elements (C, Si, Ca) might be similarly affected. The photoionization rates are probably unlikely to be seriously in error, but possible underestimation of the low temperature radiative recombination rates should be considered. The Milne relation for the rate coefficient for radiative recombination $X^+ + e \rightarrow X + h\nu$ is

$$\alpha = \frac{4\pi}{(2\pi m_e kT)^{3/2}} \frac{1}{g_{X^+} c^2} \int_0^\infty dE e^{-E/kT} \sum_j g_j (E + I_j)^2 \sigma_{pi,j}(h\nu = I_j + E), \quad (22)$$

where the sum over j is over all of the terms for the ground configuration (e.g., $2s^2 2p^2 3P$, $1D$, $1S$ for C) and all of the terms for one-electron excited configurations of the atom (e.g., $2s 2p^3 5S$, $2s^2 2p 3s^3 P$, $2s^2 2p 3s^1 P$, $2s 2p^3 3D$, ... for C), g_{X^+} is the degeneracy of the ion X^+ , g_j is the degeneracy of excited state j of the atom X , I_j is the energy required to ionize from excited state j , and $\sigma_{pi,j}(h\nu)$ is the photoionization cross section from excited state j . Equation (22) shows that the radiative recombination rate at $T \lesssim 100$ K could be large if some state j has a photoionization cross section $\sigma_{pi,j}$ with a resonance within $\lesssim 0.01$ eV of threshold. While we have no indication that such a resonance exists, we encourage atomic physicists to reexamine the calculated photoionization rates and implied radiative recombination rates. Such a near-threshold photoionization resonance, and consequent large low-temperature recombination rate, could conceivably also occur for Mg^0 .

7. ELECTRON FRACTION IN THE COLD NEUTRAL MEDIUM

In this section, we investigate the extent to which grain-assisted removal of H^+ and He^+ decreases the electron fraction x_e in the CNM. There are two separate contributions to the total electron fraction. The first is due to the ionization of metals, primarily C, by the far-ultraviolet radiation field. Since we expect C to always be primarily in C^+ in cold diffuse clouds, we simply set this contribution to $x_{e,0} \approx 2 \times 10^{-4}$. The second contribution is due to ionization (primarily of H and He) by cosmic rays and by the diffuse X-ray radiation field.

Wolfire et al. (1995) estimate the cosmic ray ionization rate for H and He (including ionization due to secondary electrons) in diffuse clouds to be $n_H \xi_{CR} \approx 3 \times 10^{-17} n_H s^{-1}$ (see their §2.2.2). They also give an approximate expression for the H and He X-ray ionization rate ξ_{XR} (for the X-ray radiation field in the local neighborhood) in terms of x_e and the column density N_w of warm gas surrounding a cold diffuse cloud (see their Appendix A). Following Wolfire et al., we adopt $N_w = 10^{19} \text{ cm}^{-2}$.

For simplicity, we assume that all of the ionization resulting from cosmic rays and X-rays comes from H;¹¹ in this case, $x_e = x_{e,0} + x_H$, where $x_H \equiv n(H^+)/n_H$. Ionization equilibrium for H is expressed by the following equation:

$$(\xi_{CR} + \xi_{XR}) n_H (1 - x_H) = (\alpha_r(B) x_e + \alpha_g) x_H n_H^2. \quad (23)$$

Here we use the ‘‘case B’’ recombination coefficient; i.e., only recombinations to states with principal quantum number $n \geq 2$ are included, since recombinations to $n = 1$ result in an ionizing photon which is immediately absorbed by a nearby H atom. We take $\alpha_r(B) = 3.5 \times 10^{-12} (T/300 \text{ K})^{-0.75} \text{ cm}^3 \text{ s}^{-1}$ (Liszt 2001).

¹¹ The rates for radiative recombination and grain recombination for $He^+ \rightarrow He$ are not very different from those for $H^+ \rightarrow H$, so the derived electron density is not very sensitive to the fraction of the ionizations that ionize H vs. He. A treatment including He would likely result in $\lesssim 10\%$ increases in n_e .

In Figure 8, we display the resulting electron fraction as a function of n_H for a range of temperatures characteristic of cold diffuse clouds (solid curves). We also show the electron fraction that would result if grain-assisted ion removal were not included in the ionization balance (dashed curves). As n_H increases, grain-assisted ion removal becomes more important and the results for x_e diverge. When $n_H = 30 \text{ cm}^{-3}$ and $T = 100$ K, grain-assisted ion removal reduces x_e from $\approx 8.0 \times 10^{-4}$ to $\approx 4.5 \times 10^{-4}$, a 45% reduction.

8. CONCLUSIONS

The principal results of this paper are as follows:

1. We define a rate coefficient α_g for the removal of ions from the gas phase due to charge exchange with grains, including PAHs (eq. 5); ‘‘removed’’ ions either remain in the gas phase, in a lower ionization stage, or stick to the grain. We compute α_g for several astrophysically important ions, as a function of the gas temperature T and grain-charging parameter ψ and provide a convenient fitting formula (eq. 8 and Table 2).
2. We evaluate a critical electron fraction x_{crit} ; if $x \equiv n_e/n_H < x_{crit}$, then grain-assisted ion removal occurs more rapidly than radiative recombination. We find that the rates for grain-assisted ion removal and radiative recombination are comparable in the CNM, but that radiative recombination dominates in the WNM and WIM (Figs. 3 and 4).
3. We provide formulae for deriving the electron density n_e from observed neutral/ionized column density ratios when grain-assisted ion removal is important, for the cases that only two ionization stages are significantly populated (eq. 15) and that three stages are populated (eqs. 16–21).
4. We have investigated whether or not grain-assisted ion removal can reconcile various estimates obtained by Spitzer & Fitzpatrick (1997) for n_e in the cold gas clouds along the line of sight to HD 215733 (§5.1). Without grain-assisted ion removal, the C and Mg determinations are consistent, while the Ca determinations are systematically lower. When grain-assisted ion removal is included, the Mg determinations are intermediate between the C and Ca determinations, and consistent with both. However, the C and Ca determinations remain inconsistent.
5. We have investigated whether or not grain-assisted ion removal can reconcile the various estimates obtained by W99 for n_e in the cold gas along the line of sight to 23 Ori (§5.2). W99 estimated n_e by observing neutral/ionized column density ratios for several elements and assuming that only ionization by the interstellar radiation field and radiative recombination are important to the ionization equilibrium. If grain-assisted ion recombination is the only additional process relevant to the ionization equilibrium, then the various n_e determinations are not reconciled. However, dissociative recombination of CH^+ may be an important recombination mechanism

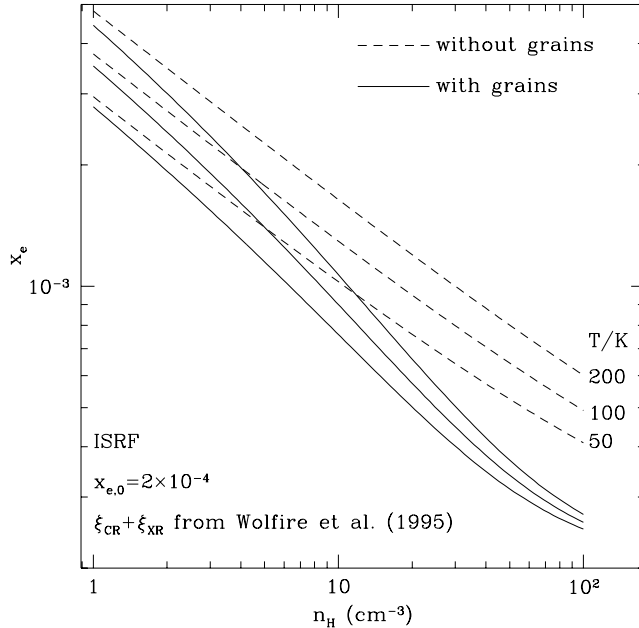


FIG. 8.— Electron fraction x_e as a function of the H density n_H . The electron fraction consists of a term $x_{e,0} \approx 2 \times 10^{-4}$ due to the ionization of metals (primarily C) by the far-ultraviolet radiation field and a term due to the ionization of H and He by cosmic rays and X-rays. Higher curves are for higher gas temperatures T , as indicated. The solid (dashed) curves were computed with (without) the grain-assisted removal of H^+ and He^+ .

for C, and the Na and K neutral/ionized ratios inferred by W99 may be incorrect, if their assumed depletions are incorrect. Making use of these degrees of freedom, we find that most of the observed abundance ratios are consistent with $n_e \approx 0.03 \text{ cm}^{-3}$. However, Mg, Si, and Ca remain discrepant, with inexplicably high neutral/ionized ratios. We have considered the possibility that the observed neutral/ion ratios for Mg, Si, and Ca might be due to an additional warm gas component with $T \approx 10^4 \text{ K}$ and $n_e \gtrsim 3 \text{ cm}^{-3}$. However, such a scenario does not appear to be consistent with the observed C^+ and Si^+ fine structure excitation. Alternatively, the enhanced abundances of Mg^0 , Si^0 , and Ca^0 could perhaps be explained if dust is being rapidly destroyed and injecting neutral Mg, Si, and Ca into the gas, but it is hard to imagine how the dust destruction could occur rapidly enough for this to be the case.

6. We suggest that low temperature radiative recombination rates might have been underestimated for Mg, Si, and Ca.

7. We have found that the grain-assisted removal of H^+ and He^+ can have a significant effect on the electron fraction in the CNM (§7). For clouds with $T \approx 100 \text{ K}$ and $n_H \approx 30 \text{ cm}^{-3}$, x is reduced from 8.0×10^{-4} to 4.5×10^{-4} . We have assumed that the ionization of C contributes an electron fraction of 2×10^{-4} .

This research was supported in part by NSF grant AST-9988126 and by an NSF International Research Fellowship to J. C. W. We thank H. Liszt, T. M. Tripp, and P. A. M. van Hoof for helpful discussions. We especially thank E. B. Jenkins and D. E. Welty for a number of valuable suggestions. We are grateful to R. H. Lupton for the availability of the SM plotting package.

APPENDIX

GRAIN-ION INTERACTION POTENTIAL

We assume that the electrostatic potential energy of an ion of charge ze at the surface of a grain with charge Ze can be approximated by a point charge ze a distance r_0 from the surface of a conducting sphere with radius a and charge Ze (see eq. [2.9] of Jackson 1962):

$$U(Z, z) = \frac{Zze^2}{a+r_0} + \frac{z^2 e^2 a^3}{2r_0(a+r_0)^2(2a+r_0)} \quad (\text{A1})$$

Then, the change in electrostatic interaction energy due to the electron transfer from grain to ion is just $\Delta U(Z, z) = U(Z+1, z-1) - U(Z, z)$ (see eq. [7]).

REFERENCES

- Aldrovandi, S. M. V. & Péquignot, D. 1974, *Rev. Bras. de Fisica*, 4, 491
Allamandola, L. J., Tielens, A. G. G. M., & Barker, J. R. 1985, *ApJ*, 290, L25
Arnaud, M. & Raymond, J. 1992, *ApJ*, 398, 394
Bakes, E. L. O., & Tielens, A. G. G. M. 1994, *ApJ*, 427, 822
Draine, B. T., & Katz, N. 1986, *ApJ*, 310, 392
Draine, B. T. & Lazarian, A. 1998, *ApJ*, 508, 157
Draine, B. T., & Li, A. 2001, in preparation
Draine, B. T. & Sutin, B. 1987, *ApJ*, 320, 803
Duley, W. W., Hartquist, T. W., Sternberg, A., Wagenblast, R., & Williams, D. A. 1992, *MNRAS*, 255, 463
Falgarone, E., Pineau des Forêts, G., & Roueff, E. 1995, *A&A*, 300, 870
Federman, S. R., Rawlings, J. M. C., Taylor, S. D., & Williams, D. A. 1996, *MNRAS*, 279, L41
Fitzpatrick, E. L. 1997, *ApJ*, 482, L199
Fitzpatrick, E. L. & Spitzer, L. 1997, *ApJ*, 475, 623
Habing, H. J. 1968, *Bull. Astron. Inst. Netherlands*, 19, 421
Jackson, J. D. 1962, *Classical Electrodynamics* (New York: Wiley)
Joulain, K., Falgarone, E., Pineau des Forêts, G., & Flower, D. 1998, *A&A*, 340, 241
Keenan, F. P., Johnson, C. T., Kingston, A. E., & Dufton, P. L. 1985, *MNRAS*, 214, 37P
Keenan, F. P., Lennon, D. J., Johnson, C. T., & Kingston, A. E. 1986, *MNRAS*, 220, 571
Kimura, M., et al. 1997, *Phys. Rev. A*, 56, 1892
Launay, J.M., & Roueff, E. 1977, *J. Phys. B10*, 879
Léger, A. & Puget, J. L. 1984, *A&A*, 137, L5
Lepp, S., Dalgarno, A., van Dishoeck, E. F., & Black, J. H. 1988, *ApJ*, 329, 418
Li, A. & Draine, B. T. 2001, *ApJ*, submitted
Lide, D. R. 2000, *CRC Handbook of Chemistry and Physics*, 81st ed. (Boca Raton: CRC Press)
Liszt, H. 2001, submitted to *A&A*[astro-ph/0103246]
Mathis, J.S., Mezger, P.G., & Panagia, N. 1983, *A&A*, 128, 212
Mezger, P.G., Mathis, J.S., & Panagia, N. 1982, *A&A*, 105, 372
Nussbaumer, H. & Storey, P. J. 1986, *A&AS*, 64, 545
Olson, R. E., Saxon, R. P., & Liu, B. 1980, *J. Phys. B13*, 297
Omont, A. 1986, *A&A*, 164, 159
Péquignot, D. & Aldrovandi, S. M. V. 1986, *A&A*, 161, 169
Pineau des Forêts, G., Flower, D.R., Hartquist, T.W., & Dalgarno, A. 1986, *MNRAS*, 220, 801
Porile, N. T. 1987, *Modern University Chemistry* (San Diego: Harcourt Brace Jovanovich)
Sellgren, K., 1994, in *The Infrared Cirrus and Diffuse Interstellar Clouds*, ed. R. Cutri & W. B. Latter, A.S.P. Conference Series, 58, 243
Shull, J. M., & van Steenberg M. 1982, *ApJS*, 48, 95
Weingartner, J. C. & Draine, B. T. 1999, *ApJ*, 517, 292
Weingartner, J. C. & Draine, B. T. 2001a, *ApJ*, 548, 296
Weingartner, J. C. & Draine, B. T. 2001b, *ApJSuppl.*, 135, 000 [astro-ph/9907251]
Weisheit, J. C., & Upham, R. J., Jr. 1978, *MNRAS*, 184, 227
Welty, D. E., & Hobbs, L. M. 2001, *ApJS*, 133, 345
Welty, D. E., Hobbs, L. M., Lauroesch, J. T., Morton, D. C., Spitzer, L., & York, D. G. 1999, *ApJS*, 124, 465 (W99)
Wolfire, M. G., Hollenbach, D., McKee, C. F., Tielens, A. G. G. M., & Bakes, E. L. O. 1995, *ApJ*, 443, 152

TABLE 1
ATOMIC DATA

Species	IP ^a eV	r_0^b	Γ_1^c s ⁻¹	Γ_2^d s ⁻¹	$\alpha_{r+d}(T = 100\text{K})^e$ cm ³ s ⁻¹	$\alpha_{r+d}(T = 6000\text{K})^e$ cm ³ s ⁻¹
H ⁰	13.60	0.37	8.61E-12	6.01E-13
He ⁰	24.60	0.50	8.42E-12	6.71E-13
C ⁰	11.26	0.77	2.0E-10	3.3E-10	8.63E-12	7.44E-13
Na ⁰	5.14	1.86	1.3E-11	1.5E-11	6.77E-12	3.00E-13
Mg ⁰	7.65	1.60	7.9E-11	7.1E-11	7.18E-12	4.66E-13
Si ⁰	8.15	1.18	3.0E-9	3.1E-9	9.39E-12	1.56E-12
S ⁰	10.36	1.03	7.8E-10	1.2E-9	7.46E-12	5.66E-13
K ⁰	4.34	2.27	5.6E-11	6.3E-11	1.11E-11	4.16E-13
Ca ⁰	6.11	1.97	3.7E-10	4.3E-10	7.07E-12	2.40E-12
Mn ⁰	7.43	1.37	1.4E-10	1.5E-10	8.33E-12	2.16E-13
Fe ⁰	7.90	1.24	2.0E-10	2.0E-10	8.52E-12	2.48E-13
Ca ⁺	11.87	1.97	1.4E-12	2.5E-12	2.70E-11	1.02E-12

^afrom Lide 2000

^bfrom Porile 1987

^cIonization rate for the WJ1 radiation field, from Péquignot & Aldrovandi 1986

^dIonization rate for the Draine radiation field, from Péquignot & Aldrovandi 1986

^eRate coefficient for radiative plus dielectronic recombination. α_r from rrfit.f (see footnote 6); α_d from Aldrovandi & Péquignot 1974 (Na⁰), Nussbaumer & Storey 1986 (Mg⁰, Si⁰), Shull & van Steenberg 1982 (Ca⁰, Ca⁺), Arnaud & Raymond 1992 (Fe⁰).

TABLE 2
FITTING PARAMETERS FOR GRAIN-ASSISTED ION REMOVAL RATE COEFFICIENT^a

Ion	C_0	C_1	C_2	C_3	C_4	C_5	C_6
H ⁺	3.436	1.909E-6	1.496	1.790E3	9.749E-4	0.5612	7.245E-5
He ⁺	2.175	2.031E-7	2.114	1.134E4	2.197E-6	1.0731	9.119E-9
C ⁺	45.58	6.089E-3	1.128	4.331E2	4.845E-2	0.8120	1.333E-4
Na ⁺	2.178	1.732E-7	2.133	1.029E4	1.859E-6	1.0341	3.223E-5
Mg ⁺	2.510	8.116E-8	1.864	6.170E4	2.169E-6	0.9605	7.232E-5
Si ⁺	2.166	5.678E-8	1.874	4.375E4	1.635E-6	0.8964	7.538E-5
S ⁺	3.064	7.769E-5	1.319	1.087E2	3.475E-1	0.4790	4.689E-2
K ⁺	1.596	1.907E-7	2.123	8.138E3	1.530E-5	1.0380	4.550E-5
Ca ⁺	1.636	8.208E-9	2.289	1.254E5	1.349E-9	1.1506	7.204E-4
Mn ⁺	2.029	1.433E-6	1.673	1.403E4	1.865E-6	0.9358	4.339E-9
Fe ⁺	1.701	9.554E-8	1.851	5.763E4	4.116E-8	0.9456	2.198E-5
Ca ⁺⁺	8.270	2.051E-4	1.252	1.590E2	6.072E-2	0.5980	4.497E-7

^aSee eq. (8).

TABLE 3
INFERRED TEMPERATURES AND HYDROGEN NUMBER DENSITIES FOR COLD CLOUD COMPONENTS TOWARDS HD 215733^a

Component	T K	n_{H} cm ⁻³
7	240	22
11	100	13
12	240	5
13	110	23
15	130	21
16	100	10
17	100	18
18	50	24
19	100	10

^aFrom Fitzpatrick & Spitzer 1997.